PhDay Físicas 2019

1. Evolution of hydrogen-rich exospheres around Earth-like exoplanets

Ada Canet Varea

The presence of hydrogen-rich atmospheres around Earth-like exoplanets could be a reliable tracer of water and other volatile elements near the planetary surface. Recently, observations of the Earth in the ultraviolet range have shown that our planet's exosphere is much more extense than previously thought, suggesting that it could be a common feature in other rocky extrasolar planets. Hydrogen dominated extended exospheres (EEs) have been widely modeled and detected in giant, gaseous exoplanets. However, their detection around smaller, rocky planets is still not achieved, and calls for a more detailed modeling. The evolution and stability of such these exospheres strongly depends on the radiation, magnetic fields and particle flow coming from the host star, i.e. stellar winds. In order to address these star-planet interactions, we carried out numerical 2.5D MHD simulations using the PLUTO code, to show how the H-rich EE of an Earth-like planet evolves at different stellar ages (from a very young, solar-like star of 0.1 Gyr to a 5 Gyr star), and to study its stability according to the hydrogen density initially present in the planet's EE. Our simulations indicate that hydrogen atmospheres of planets orbiting more evolved stars are more susceptible to be detected. The stellar age-dependent evolution of H-rich atmospheres obtained in this work allows us to determine the optimal targets to observe in order to detect H-rich EEs around rocky exoplanets, those being promising candidates to host water in their lower atmospheres.

2. Experimental and numerical evaluation of drift errors in a solar power tower facility with tilt-roll tracking-based heliostats

Alejandro Martínez Hernández

Solar power tower facilities make use of sun-tracking mirrors, called heliostats, to focus solar radiation in a specified aiming point on a target. In this context, a relevant problem to be tackled is the deviation of the focused solar beam with respect to the aiming point along the time of the day, known as drift. In this work, we experimentally and numerically evaluate the drift errors in a solar tower facility with tilt-roll tracking-based heliostats. For this investigation, the solar power tower facility located at IMDEA Energy in Móstoles (Spain) is used as a test case. By acquiring flux maps at different times of the day and representing their maximum irradiance point as a function of the time, the drift is evaluated experimentally. We observed that the experimental drift can be divided in two components, vertical and horizontal, with a constant velocity of the maximum irradiance point of -7.4 cm/h and 2.2 cm/h, respectively. In order to investigate the source of the drift observed in the experiment, detailed Monte Carlo ray-tracing simulations including possible misalignments in the heliostat tracking system were performed. We found out that by considering rotations of the heliostats pedestal, the experimental drift is very well reproduced by the simulations. In particular, for a rotation of the pedestal of 17 mrad towards the east, the velocities of the maximum irradiance point in the simulations are -7.6 cm/h and 1.1 cm/h for the vertical and horizontal drift components, respectively.

3. Synthesis and characterization of doped SnO2 and TiO2 nanoparticles and hybrid composites for technological applications

Antonio Vázquez-López

Wide-bandgap semiconductor oxides as SnO2 or TiO2 have demonstrated potential applications [1] in diverse fields of technological research ranging from catalysis, photovoltaic applications or energy storage as Lithium ion batteries. For these purposes controlled morphology and size of the nanaoparticles as well as appropriate doping are necessary.

Besides, combination of these inorganic nanomaterials (SnO2, TiO2) with organic materials such as PEDOT:PSS (transparent conductive polymer) to form hybrid composites [2] can lead to enhanced performance and advantages due to the synergy between its two counterparts. Actually, hybrid composites are one of the most promising candidates for the new photovoltaic technology based on clean, low cost and flexible devices.

In this work, SnO2 and TiO2 nanoparticles, undoped and doped with Li or Ni, were synthesized by hydrolysis. A morphological and structural (XRD, TEM), vibrational (Raman) and luminescence (Photoluminescence) characterization of the samples has been performed. Moreover a surface chemical and electrical characterization (XPS, XAS) and a compositional study (EDX, ICP-OES) were also performed to determine their properties, in which a chemical structure stability even after dopant inclusion arises, while other properties such as vibrational or luminescence strongly depend of the dopant inclusion.

After the subsequent characterization, diverse optoelectronic applications were evaluated. Firstly we combined SnO2 nanoparticles to form anodes for Lithium-ion batteries and studied their capacity over time of cycles, as the use of inorganic materials as anodes can reach enhanced capacitance. On the other hand, TiO2 nanoparticles were combined with PEDOT:PSS and deposited via spin coating on n-type silicon to form hybrid p-n junctions, in which charge carriers lifetime, Si surface passivation and sheet resistance, among other properties, were studied for a possible implementation on hybrid solar cell devices.

[1] F. del Prado, A. Cremades, D. Maestre, J. Ramírez-Castellanos, J.M. González-Calbet and J. Piqueras, *J. Mater. Chem. A*, 2018, **6**, 6299-6308

[2] M García-Tecedor, S. Z. Karazhanov, G. C. Vásquez, H. Haug, D. Maestre, A. Cremades, M. Taeño, J. Ramírez-Castellanos, J.M. González-Calbet, J. Piqueras, C.C. You, E. S. Marstein, *Nanotechnology,* 2018, **29**, 035401

4. Nano-electrodes fabrication to perform electric neuronal activity measurements

Beatriz Loreto Rodilla González

Neural electrodes are devices that, directly in contact with neural tissue, can record the neural activity and trigger it through electrical stimulation. These neural electrodes can be used, for example, in the treatment of neural diseases as Parkinson, as spinal cord stimulators, cortical electrodes or retina implants, etc.

Nowadays, these electrode-based devices present size, morphology and rigidity issues that unleashes an immunologic response that inactivates them. In this work, we present metallic flexible electrodes composed by a flexible Au thin sheet with one of its faces covered by a network of metallic vertical nanowires (NWs) that we grow using template-assisted electrodeposition. To warranty a good neural electric response minimizing the damage to the surrounding tissue, a meticulous control of the geometry of the nanostructure is needed.

Using polycarbonate or anodic aluminium oxide (AAO) templates, we can tailor the nanostructure, varying the order, interdistance and diameter of the NWs. In the electrodeposition process, we can control their length and choose the material of these NWs. Also, we have developed a technique to produce core-shell NWs through pulsed electrodeposition, combining the properties of different metals.

We have obtained positive in vitro biocompatibility results of the nanostructured electrodes and the neural electric stimulation measurements performed show that our interfaces are able to trigger neural activity at low voltages. Simulations of electric field produced at an applied voltage, show that our nanostructured interfaces are expected to concentrate the electric field at the tip of de nanowires, what implies that less voltage is needed to trigger the neural electric stimulation comparing with plane electrodes. Our results support the potential of our nanostructured interfaces as flexible and compact functional electrodes.

This project has received funding from the EU Horizon 2020 R&I programme under grant agreement 737116.

5. Estimation of radiated energy for deep earthquakes

Carolina López Sánchez

The occurrence of very deep earthquakes (h>600 km) is a characteristic of the subduction regions and their origen is a question that remains open. A special case is the southern Spain (Granada region) where from 1954 five very deep earthquakes (h≈650 km) with magnitudes between 4.4 and 7.8 have occurred. The most recently deep earthquake was on 11th April 2010 with depth 623 km and magnitude Mw 6.2. In this study, we estimate its radiated seismic energy (Es) in order to understand the rupture process. The method that we have used is based on the direct integration of P wave waveforms. We have selected seismograms recorded at teleseismic (35 stations) and regional distances (72 stations). We have obtained energy values ranging from $6.00x10^{12}$ J to $1.31x10^{14}$ J with an average value of $(1.65\pm1.01)x10^{13}$ J for teleseismic distances and $3.28x10^{12}$ J to $4.96x10^{14}$ J with an average value of $(5.24\pm1.03)x10^{13}$ J for regional distances. These values have been compared with these of other recently occurred on Peru-Brazil and Fiji-Islands in 2018. From these results we have studied the relation Es/MoS versus depth.

6. Dark photon searches with atomic transitions

Clara Álvarez Luna

Dark matter could be made up of dark photons, massive but very light particles whose interactions with matter resemble those of usual photons but suppressed by a small mixing parameter. We analyze the main approaches to dark photon interactions and how they can be applied to direct detection experiments which test different ranges of masses and mixings. A new experiment based on counting dark photons from induced atomic transitions in a target material is proposed. This approach appears to be particularly appropriate for dark photon detection in the meV mass range, extending the constraints in the mixing parameter by up to eight orders of magnitude with respect to previous experiments.

7. Microwire arrays as tuneable electromagnetic absorber metamaterial.

Diego Archilla Sanz

In present work, short pieces of ferromagnetic amorphous microwires forming an array are studied as electromagnetic absorber metamaterial at microwave frequencies. Ferromagnetic amorphous microwires can be treated as electric dipoles induced by a high-frequency electric current generated by an electromagnetic field. An interesting property of this kind of materials is the magneto-electric coupling, the polarization of the microwire depends on the magnetization of the sample and can be changed in response to an external magnetic field. At the dipole resonance frequency, related with the length of the microwire, part of the electromagnetic energy is absorbed by the microwire. A study of how affect the interaction between microwires in the electromagnetic absorption have been carry out, obtaining up to -50dB of absorption (99.999% of absorption) for an array of 90 microwires, and the possibility of tune the absorption and the resonance frequency both with the number of microwires and with an external magnetic field.

8. Awake Preclinical Brain PET Imaging based on Point Sources

Fernando Arias Valcayo

The presence of motion during the relatively long PET acquisitions is a very common problem, especially with awake animals, infants and patients with neurological disorders. External motion can be detected based on the optical tracking of markers placed on the skin of the patient, but it needs additional hardware and a somehow complex integration with the PET data. The possibility of motion detection directly from the acquired PET data would overcome these limitations. In this work, we propose the use of the centroid of lines of response to identify long motion free frames (more than 2.5 seconds). Then, thanks to the high sensitivity of PET detectors, we can split these no-notion frames into smaller frames, in order to identify the motion with higher precision. In these frames we identify in real-time the location of ^{18}F markers placed on the head of the rat with the radiotracer labeled with ^{18}F. We evaluated the performance of the proposed method in a preclinical PET/CT scanner with an awake rat injected with 600 µCi and four ^{18}F sources attached in its head. After solid rigid motion compensation, we reconstruct an image that use 70% events of the acquisition, and the resolution is comparable with the motion-free frames.

9. Morphological changes of human crystalline lens in myopia

Geethika Muralidharan

Purpose: To assess relationships between ocular biometric parameters, including crystalline lens full shape, and refractive error, using 3-D quantitative Optical Coherence Tomography (OCT).

Methods: The study was performed on 21 subjects (21-37 y/o; spherical error: -6.25D-0.5D). Biometry of full anterior segment was obtained with custom-developed 3-D spectral OCT coupled with dedicated image processing algorithms. Association between anterior chamber depth (ACD), radius of curvature of anterior cornea (RAC), anterior lens (RAL), and posterior lens (RPL), lens thickness (LT), equatorial diameter (DIA), surface area (LSA), equatorial plane position (EPP), volume (VOL) and lens power (PL) was evaluated as a function of refractive error (RE) and axial length (AL) while controlling for age effects.

Results: ACD (-0.05 mm/D), DIA (-0.09 mm/D), RPL (-0.182 mm/D) and LSA(-1.71 mm2/D) increased significantly ($p<0.05$) and PL decreased (0.58 D/D) with increasing negative RE (i.e. with the magnitude of myopia); ACD (0.12 mm/mm), DIA(0.15 mm/mm), RPL(0.36 mm/mm), LSA (2.82 mm2/mm) and RAL (0.97 mm/mm) increased significantly with AL. LT (-0.12 mm/mm), EPP (-0.12 mm/mm) and PL (-1.24 D/mm) decreased with AL. VOL and RAC were not significantly correlated with RE or AL. RPL had the most influence in reduction of lens power with increasing AL than any other lens biometric parameter.

Conclusions: The crystalline lens appears to undergo changes with myopia consistent with lens thinning, equatorial and capsular stretching, while keeping constant volume. Axial elongation appears to some extent counteracted by a crystalline lens power reduction, suggesting an active role by the lens, and not only passive physical changes accompanying eye growth.

10. Magnetic properties and heating performances of magnetic nano and micro materials subjected yo radiofrequency fields and their applications

Irene Morales Casero

Magnetic nanomaterials attract a huge interest due to their properties and potential application in different fields such as biology, catalysis, contaminant removal and magnetic and energy storage. In the field of the biology, magnetic fluid hyperthermia takes advantage on the properties of superparamagnetic nanoparticles, usually iron oxide nanoparticles, to deliver localized heat on tumors, destroying cancer cells in a less invasive and more selective way than other treatments. For that purpose, a better understanding of the heating mechanisms and the clue parameters to achieve and optimized treatment has to be done.

We present a study of different iron oxide nanoparticles with sizes ranging from 6 nm to 35 nm making a deep understanding of their dynamic magnetic behaviour when subjected to alternating magnetic fields of around 100 kHz and their heating mechanisms. Their application as nanoheaters in magnetic hyperthermia with patient-derived colorectal cancer organoids has also been investigated.

Following the line of the magnetic materials and their ability to heat, we have also done a systematic study of the colossal heating performance of soft magnetic microwires subjected to alternating magnetic fields and an explanation of the origin of their heating losses is given. This colossal heating is reached with very low power supply, which makes these materials very promising for inductive heating applications at a very low energy cost.

11. Fast-timing studies of 133 Sn and 134 Sn excited states

Jaime Benito García

Exotic Sn isotopes with a few neutrons more than doubly magic 132 Sn mass are excellent cases to study nuclear properties around shell closures. In this work, excited states in 133,134 Sn isotopes were investigated by popullating them during the beta decay of 133-135 In isotopes. This investigation was performed in the framework of the IS610 at the ISOLDE-CERN facility where In was produced by spallation neutrons in a thick UCx target, selectively ionized by the ISOLDE Resonance Ionization Laser Ion Source, mass separated and transported to the ISOLDE Decay Station. The latter was equipped with four high-efficiency clover-type Ge detectors, and a compact set-up for fast timing studies consisting of a plastic beta-particle detector and ultrafast LaBr 3 (Ce) scintillation detectors.

In this work we focus in the study of the lifetimes. The excited structure of 134 Sn had been earlier investigated in 248C m spontaneous fission experiments [1]. The observation of the cascade of three gamma-rays of 174, 348, and 726 keV led to the identification of three excited levels at 1247, 107 and 726 keV as the three states arising from the two-neutron seniority scheme (vf 7/2) 2 with 6 + ,4 + ,2 + spin-parity. In this work, those levels were studied from the ß decay of 134 In as well as from the ß-n decay of 135 In. The high yields achieved during IS610 experiments allowed us to perform a complete fast-timing investigation carried out over those three levels. We report on the new half-lives measured in this work three levels, from whose the B(E2) transition rates were derived.

In addition we have also studied lifetimes in 133 Sn. Its excited structure was already investigated from the beta-decay of 133 In [2]. In this work, we report on the lifetime measurement of the 854-keV single particle state with p 3/2 dominant configuration compared with the previous value obtained at RIKEN [3].

[1] A. Korgul *et al.* , Eur. Phys. J. A 7, 167 (2000).
[2] M. Piersa *et al.* , Phys. Rev. C 99, 024304 (2018).
[3] V. Vaquero *et al.* , Phys. Rev. Lett. 118, 202502 (2018).

12. Zn2GeO4, a promising material in optoelectronic applications and energy reserve

Jaime Dolado Fernández

Transparent conducting oxides (TCO's), which exhibit both high electrical conductivity and high optical transparency in visible light, are necessary for a variety of optoelectronic applications [1]. Not only binary but also ternary oxides have been explored as TCO materials, being Zn2GeO4 with a wide-bandgap (4.7 eV) one of the most appealing. Besides the optical transparency Its crystalline structure consists of corner-shared ZnO4 and GeO4 tetrahedra forming six-member rings with room enough for interstitial atoms. This configuration made Zn2GeO4 a promising material for application in metal-ion batteries as a high-capacity anode material. On the other hand, native defects usually play a fundamental role in the physical properties in semiconducting oxides, e.g. optical properties, photocatalytic properties or ionic transport, which is very important for batteries. The native defects in Zn2GeO4 are oxygen vacancies and zinc interstitials, with a donor character, and zinc and germanium vacancies as acceptors. They are responsible for the luminescence spectra observed in Zn2GeO4 [2,3].
In this PhD thesis, we study the correlation between luminescence and structural properties in undoped and doped Zn2GeO4 samples. The intense white luminescence of Zn2GeO4 nanomaterials makes them of interest as efficient phosphors for field emission displays. The luminescence results support the incorporation of light elements, such as Mg or Li, as interstitial ions which could be used for metal-ion batteries applications. In addition, we have explored the formation of nanowire-based heterostructures based on Zn2GeO4 nanowires and SnO2 particles and proposed models for the growth mechanism. [4].

References

[1]. Hosono, H. et. al., "A germanate transparent conductive oxide". *Nature Communications* **2011,** *2*, 470.

[2]. Hidalgo P. et al., "Synthesis and optical properties of Zn2GeO4 microrods," Acta Mater., **2016**, vol. 104, pp. 84–90.

[3]. Dolado J. et. al., "Correlative study of vibrational and luminescence properties of Zn2GeO4 microrods". Physica Status Solidi (a) 2018, 215(19), 1800270.

[4]. Dolado J. et. al., "Zn2GeO4/SnO2 nanowire heterostructures driven by Plateau-Rayleigh instability". Nano Letters (under review).

13. Chalcogenides and skutterudites as thermoelectric materials: Structural information and improvement of their thermoelectric properties

Javier Gainza Martín

Thermoelectric materials are outstanding to transform temperature differences directly and reversibly into electrical voltage. Exploiting waste heat recovery as a source of power generation could help to move towards an energy sustainability future. Thermoelectric materials are characterized by the thermoelectric figure of merit, $ZT = \frac{\sigma S^2}{\kappa} T$, combining into a dimensionless number the Seebeck coefficient, S, the electrical conductivity, σ, the thermal conductivity, κ, and the absolute temperature, T[1].

SnSe semiconductor was identified, in single-crystal form, as a mid-temperature thermoelectric material with record high figure of merit, high power factor and surprisingly low thermal conductivity. A further reduce of this thermal conductivity can be achieved by nanostructuring[2] and, at the same time, doping can be used to increase σ, so the ZT value could be improved compared to the pure tin selenide.

GeTe presents an extremely high electrical conductivity and hole carrier concentration due to the Ge vacancies in the structure. To optimize it, it is usually doped with Bi or Sb, reducing the number of hole carriers and increasing the mass fluctuation effect to reduce the lattice thermal conductivity. Moreover, modifying its crystal structure leads to a higher degeneracy in band valleys, yielding an even higher thermoelectric performance.

$CoSb_3$ skutterudites are tellurium- and lead-free materials with a complex $CoAs_3$-like structure and promising thermoelectric properties. Pristine CoSb3 and filled skutterudites $R_xCo_4Sb_{12}$ (R = K, Sr, La, Ce, Yb, Mm) (Mm=La+Ce) have been synthesized and sintered in one step under high-pressure conditions at 3.5 GPa in a piston-cylinder hydrostatic press. We have characterized the structural properties of the reaction products by synchrotron x-ray diffraction and high resolution TEM.

Filled compounds diffraction patterns clearly show an uneven filling fraction of the skutterudite phases, confirmed by transmission electron microscopy. This non-homogeneous distribution of R filling atoms is adequate to produce a significant decrease in lattice thermal conductivity, mainly due to strain field scattering of high-energy phonons[3]. Besides that, filler atoms contributed to increase the charge carrier concentration in the samples, as well as an enhancement of the power factor.

References

1. Snyder, G. J. & Toberer, E. S. Complex thermoelectric materials. *Nat. Mater.* **7**, 105–114 (2008).

2. Gainza, J. *et al.* Evidence of nanostructuring and reduced thermal conductivity in n-type Sb-alloyed SnSe thermoelectric polycrystals. *J. Appl. Phys.* **126**, 045105 (2019).

3. Gainza, J. *et al.* Substantial thermal conductivity reduction in mischmetal skutterudites Mm x Co 4 Sb 12 prepared under high-pressure conditions, due to uneven distribution of the rare-earth elements. *J. Mater. Chem. C* **7**, 4124–4131 (2019).

14. How climate change is affecting the patterns of electricity demand in Spain

José Manuel Garrido Pérez

Climate change is one of the main concerns worldwide due to its environmental and socio-political implications. It impacts many sectors of our society, such as health, tourism, agriculture or energy. In particular, the need to balance electricity supply and demand has become an important international policy concern in a context of growing world energy consumption. On the one hand, the supply has received considerable attention. The market is tending to move away from fossil fuels to renewable energies in order to decarbonize the energy system and decrease greenhouse gas emissions. However, there has been little quantitative analysis about how the regional patterns of electricity demand will change under global warming.

Temperature is the main meteorological driver of the day-to-day variability of electricity demand. Both cold and warm days are associated with high electricity demand due to the use of electricity heating appliances and cooling systems, respectively. Consequently, the Spanish energy system is characterized by a seasonal cycle of electricity demand with two relative maxima in winter and summer. Nowadays, the occurrence of extreme electricity demand days is higher in winter than in summer, but this may change with the projected increase in temperatures over the twenty-first century. This work analyses the expected future demand in Spain by using projected temperatures from climate models and an observational demand-temperature relationship. The main results point to a widening of the distributions of daily electricity demand and a seasonal shift of extreme electricity demand days from winter to summer. These results have clear implications for the electricity pool design and may help policy makers in the energy management system.

15. Nonclassicality as an alternative resource for quantum metrology

Laura Ares Santos

Quantum fluctuations impose fundamental limits to the sensitivity of the detection of weak signals. The aim of our work is to optimize detection processes to increase the sensitivity achievable for fixed resources. We analyze a general metrological scheme where the signal to be measured is encoded by a different transformation in each case, and the Fisher Information is used to quantify the minimum variation detectable [1]. We have seen that energy could be a not as convenient resource as it was thought [2]. Contradictory results in the relation between the energy involved and the minimum uncertainty achievable have been found for linear transformations. We examine whether nonclassicality is a more useful account of resource [3]. Moreover, for completeness we include all the resources employed in the full measurement process including the final measurement performed. We specifically use gaussian states for modeling both probe and detector states for their practical value and in order to easily quantify the nonclassicality. In addition, we analyze the contribution of the squeezing of measurement states to the total amount of nonclassicality of the process finding an optimum relation to the squeezing of the probe state.

[1] L. Motka et al., Eur. Phys. J. Plus 131, 130 (2016).
[2] A. Luis, Phys. Rev. A 69, 044101 (2004).
[3] H. Kwon, K. C. Tan, T. Volkoff, and H. Jeong, Phys. Rev. Lett. 122, 040503 (2019).

16. Variación de la ley de extinción ultravioleta en las envolturas de las nubes moleculares. Acoplamiento magnético al campo Galáctico.

Leire Beitia Antero

Las nubes moleculares son las grandes factorías donde tiene lugar la formación estelar. El tipo de estrellas que formará en su interior depende tanto de la masa de la nube como del estado turbulento del gas, así como de la capacidad de penetración de los campos magnéticos. Las capas más externas de las nubes moleculares son más difusas, y al estar sometidas a la radiación ultravioleta externa, se ionizan, favoreciendo el acoplamiento con el campo magnético y la propagación de ondas hidromagnéticas a su interior. En este proceso, los granos de polvo acoplados al gas juegan un papel fundamental, ya que también poseen una carga neta que provoca su oscilación alrededor de las líneas de campo magnético. Así, algunas de las ondas que se propagan en la nube pueden verse amplificadas al entrar en resonancia con los granos de polvo cargados, aumentando el estado turbulento de la nube y disminuyendo el tamaño de las estrellas que se formarán en su interior. Para estudiar numéricamente esta fenomenología, hemos modificado un código de simulación magnetohidrodinámica para incluir la dinámica de los granos cargados. En este trabajo, presentamos los resultados obtenidos hasta la fecha sobre la amortiguación de las ondas en presencia de granos de polvo de 0.01 micras de radio.

17. Materiales compuestos basados en óxido de galio

Marina García Carrión

En los últimos años se ha visto incrementado el estudio de nuevos materiales para aplicaciones en energía. Uno de los materiales semiconductores más estudiados actualmente con ese objetivo es el óxido de galio. Sus características, como son su banda de energía prohibida (*band gap*) muy ancha y el campo de ruptura (*breakdown field*), le aportan ventajas sobre otros materiales funcionales a la hora de utilizar ciertas propiedades ópticas y electrónicas por medio del diseño de defectos.

Este trabajo se estructura en dos líneas de investigación. Una de ellas es el estudio de nanocristales de dos fases de óxido de galio, *β*-Ga_2O_3 y *γ*-Ga_2O_3, obtenidas mediante síntesis química. La primera fase, beta, es muy conocida desde hace varias décadas por ser la más estable de las fases cristalinas de este compuesto. Investigar las propiedades de la fase gamma a nanoescala es de gran importancia para entender sus características únicas para potenciales aplicaciones en energía.

La otra línea de investigación se enfoca en la serie homóloga $Na_xGa_{4+x}Ti_{n-4-x}O2_{n-2}$ (beta-galia-rutilo, $x \approx 0.7$, $n > 4$). En este trabajo se han sintetizado los tres primero términos de la serie, n = 5, 6 y 7. Este material resulta del intercrecimiento ordenado de unidades *β*-Ga_2O_3 (tetraédricas y octaédricas) con unidades octaédricas de TiO_2, dando como resultado una estructura cristalina con túneles definidos a lo largo de una dirección cristalográfica. Esta característica lo convierte en un material con gran potencial para aplicaciones de conducción iónica, entre otras.

En este trabajo, además de la síntesis de los materiales mencionados, se ha llevado a cabo el estudio experimental de sus propiedades luminiscentes así como de su estructura cristalina y su morfología. Tanto el *band gap* como las bandas de luminiscencia de los tres términos beta-galia-rutilo han mostrado interesante propiedades mediante técnicas de luminiscencia. Las nanopartículas de óxido de galio se han implementado en PEDOT:PSS, material orgánico base para la fabricación de placas solares híbridas, caracterizando las propiedades optoelectrónicas de dicho *composite*.

18. Magnetic phase diagram of nanostructured zinc ferrite as a function of inversion degree δ

Miguel Ángel Cobos Fernández

Massive Zn ferrite has a normal spinel structure (with all Zn^{+2} cations in the tetrahedral (A) sites, while Fe^{+3} cations occupy the octahedral (B) ones), and it behaves paramagnetic at room temperature. Stoichiometric $ZnFe_2O_4$ was synthesized from a powder mixture of ZnO and Fe_2O_3 at 99% by high energy mechanical milling in air. Microstructural characterization of resulting material by XRD confirmed the presence only of zinc ferrite after 150h milling and the Rietveld refinement of this spectrum showed a cation inversion close to 0.60, which was associated with a random distribution of Zn^{2+} and Fe^{3+} cations over tetrahedral and octahedral sites.

It has been reported that synthetic and processing methods can have a significant influence on the physical properties of spinel since it can produce a metastable disordered structure. In this case, the structural formula must be written as $(Zn_{1-\delta}Fe_{\delta})[Zn_{\delta}Fe_{2-\delta}]O4$, where δ represents the degree of inversion (defined as the fraction of A sited occupied by Fe cations). This redistribution of Zn^{2+} and Fe^{3+} cations leads to the onset Fe^{3+} - Fe^{3+} magnetic interaction between A-B sublattices.

The as-milled samples, with a high inversion degree were subjected to different thermal annealing from 300 to 600 ºC, where inversion degree (δ) decreases from 0.55 to 0.18. A magnetic phase diagram as a function of δ can be inferred from the results: 1) for δ<0.25, Antiferromagnetism (AFM), Ferrimagnetism (FiM) and Spin Glass (SG) behaviors were observed to coexist, 2) for 0.25<δ<0.5, the FM clusters coalesced and SG behavior vanished remaining only a pure FiM phase with a maximum magnetization of M_s = 3.5 μ_B. Finally, 3) for δ>0.5, There is a FiM and AFM coexistence, where this AFM is given by compensated spins in the J_{AB} interactions.

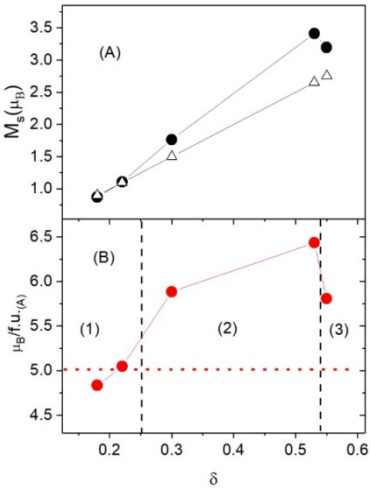

Figure: (A) saturation magnetization per Bohr magneton as a function inversion degree δ (black circles) and saturation calculated as $M_s = \delta(5\mu_B)$(open triangles). (B) Saturation magnetization per ferromagnetic unit (f.u.) at A sites. The regions (1), (2) and (3) indicate FiM+AFM+SG, FiM and FiM+AFM phases, respectively

19. Impact of improved land model depth and hydrology on climate change projections.

Norman Steinert

The representation of the thermal and hydrological state in Land Surface Models is crucial to have a realistic simulation of subsurface processes and the coupling between the atmo-, lito and biosphere. There is evidence suggesting an inaccurate simulation of subsurface thermodynamics in current-generation Earth System Models, which have land model components that are too shallow. In simulations with a bottom boundary too close to the surface, the energy propagation and spatio-temporal variability of subsurface temperatures are distorted. This impedes the simulation of land-air interaction and subsurface phenomena, e.g. energy/moisture balance and storage capacity, freeze/thaw cycles and permafrost evolution.

We introduce modifications for a deeper soil into the MPI Earth System Model for climate projections of the 21st century. The depth-changes in the soil have implications for the hydrological regime, in which the moisture between the surface and the bedrock is sensitive to depth changes in the thermal regime. Additionally, we introduce different soil hydrological states, with major implications for vertical soil moisture distribution and its exchange with the land surface. They influence the representation of permafrost and the interaction of soil moisture and energy. Overall, we explore the sensitivity of our results to an improved soil thermal and hydrological state with the help of 1) an evaluation of the soil thermodynamic aspects and 2) the simulation of permafrost areas in the Northern Hemisphere high latitudes.

The latter is of particular interest due to their vulnerability to long-term climate change. They represent one of the tipping elements of the Earth's climate system that decisively drive the agreement of future carbon emission targets.

20. Nano-dispersion-scan: Measurement of sub-7 fs laser pulses using second-harmonic nanoparticles

Óscar Pérez Benito

Ultrashort laser pulses play nowadays a fundamental role in different fields, such as high-energy physics, time-resolved measurements in matter or bioimaging. Hence, a complete characterization of the pulse amplitude and spectral phase is of key importance both to control and to use them in different physical systems.

A recent, and especially suitable technique to measure pulses below 10 fs is dispersion-scan (d-scan). Here the spectral phase of the fundamental pulse is modified in a controlled way using a compressor block made of negatively chirped mirrors and a pair of glass wedges. Focusing these series of pulses onto a nonlinear system, for example a second-harmonic (SH) crystal, a set of different SH spectra can be recorded as a function of glass insertion, thus drawing a d-scan trace. Suitable algorithms have been developed to retrieve the spectral phase and the temporal profile of the fundamental pulse from these traces. SH crystals have certain limitations due to phase-matching requirements: they are specific for a certain spectral zone, they must be only several microns thick to be used with broadband pulses, and hence they are expensive.

In this work, we demonstrate that house-made ensembles of commercially available low-cost barium-titanate ($BaTiO_3$) nanoparticles (NPs) can be employed not only to generate a strong SH signal, but also to record d-scan traces. Due to the size of the nanoparticles, scattering plays an important role in SH generation by adding an incoherent component to the d-scan trace (while bulk crystals, in contrast, generate fully coherent SH signals). We have modified the standard algorithm to calculate the coherent and incoherent contributions to the trace and to deduce the correct pulse duration (known from measurements with a bulk crystal). With this new algorithm a whole variety of traces differing in the coherent content of the signal could be retrieved, showing the robustness of the measuring and retrieving procedures.

Since NPs are not subject to phase-matching conditions, these results pave the way to using NPs to characterize ultrashort pulses in any spectral range, from the infrared to the ultraviolet, at a very low cost.

21. A Quantum Interior-Point Predictor-Corrector Algorithm for Linear Programming

Pablo Antonio Moreno Casares

We introduce a new quantum optimization algorithm for dense Linear Programming problems, which can be seen as the quantization of the Interior Point Predictor-Corrector algorithm (1) using a Quantum Linear System Algorithm (2). The (worst case) work complexity of our method is, up to polylogarithmic factors,

$$O\left(L\sqrt{n}\,(n+m)\overline{||M||}_F\bar{\kappa}^2\varepsilon^{-2}\right),$$

for n the number of variables in the cost function, m the number of constraints, ε^{-1} the target precision, L the bit length of the input data, $\overline{||M||}_F$ an upper bound to the Frobenius norm of the linear systems of equations that appear, and $\bar{\kappa}$ an upper bound to the condition number κ of those systems of equations. This represents a quantum speed-up in the number n of variables in the cost function with respect to the comparable classical Interior Point algorithms when the initial matrix of the problem A is dense and we substitute the quantum part of the algorithm by classical algorithms such as Conjugate Gradient Descent, what would mean the whole algorithm has complexity $O\left(L\sqrt{n}\,(n+m)^2\bar{\kappa}\log(\varepsilon^{-1})\right)$, or with exact methods, at least $O\left(L\sqrt{n}\,(n+m)^{2.373}\right)$.Also, in contrast with any Quantum Linear System Algorithm, the algorithm described in this article outputs a classical description of the solution vector, and the value of the optimal solution. Finally, the dependence on the target precisión can be lowered to poly $log(\varepsilon^{-1})$, if the last (constant number of) iterations are performed classically.

References

[1] Y. Ye, M. J. Todd, and S. Mizuno, \An o$\sqrt{n}l$-iteration homogeneous and self-dual linear programming algorithm," Mathematics of Operations Research, vol. 19, no. 1, pp. 53-67, 1994.
[2] L. Wossnig, Z. Zhao, and A. Prakash, “Quantum linear system algorithm for dense matrices," Physical review letters, vol. 120, no. 5, p. 050502, 2018.

22. Systematic search for gamma-ray periodicity in Fermi-LAT AGN

Pablo Peñil del Campo

Blazar emissions present an intrinsic variability covering the entire range of wavelengths. Understanding the processes behind such variability will provide a better view about the nature of these extragalactic objects. However the observation of periodicities in the gamma-ray light curves of blazars is still challenging. Despite the fact that there have been individual efforts, a systematic search that considers large blazar populations is still missing. In this paper, we use ten years of gamma-ray data provided by the Fermi Large Area Telescope (LAT) to systematically study the light curves of more than two thousand AGN included in the Fermi-LAT catalogues. We use several techniques in order to find evidence of periodic emission in gamma-rays. These techniques are organized in a Periodicity-Search flow to automatize the detection of candidates to have periodicity. After analyse our AGN subsample, we have found 23 AGN with high-significant evidence of periodicity, where 18 are new periodic-emission candidates.

23. Magnetic field influence on magnetomechanical coupling of partially bistable magnetic materials

Papa Gorgui Birame Gueye

The great sensitivity to small fields makes soft magnetic materials excellent for magnetic field sensing. The magnetic material used in this work are FeSiB based magnetic microwires and ribbon obtained by Taylor's technique and their magnetostriction constant can be positive or negative depending on the Fe/Co percentage. Amorphous magnetic microwires AWM are continuous filaments with a magnetic core covered by a glassy outer shell. [1] Generally, the total diameter is less than 100 µm and the diameter of the metallic core is between 4 to 60 µm. The magnetoelastic resonance is due to the rotation of the magnetization when a material is exposed to AC magnetic field of a certain frequency. [2] Many applications are done in this way as like as: The detection of salmonella on fresh produce [3], Electronic article surveillance (EAS) alarm systems (anti-theft tags) [4], Magnetic nanodiscs for cancer therapy. etc….

The aim of this work is to study the evolution of resonance frequency of our magnetoelastic element inmmersed in different solutions.

It should be remarked that the amplitude of the resonance frequency depends on the viscosity but the frequency change is related to the additional mass added to the sensor surface.

The fundamental resonant frequency under longitudinal vibration is expressed as:

$$f = \frac{1}{2L}\sqrt{\frac{E}{\rho(1-\nu)}}$$

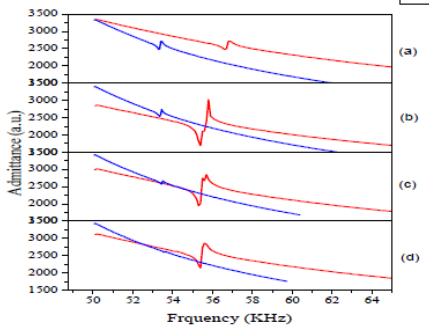

Fig.1: Spectrum resonance for (■) wire, (■) ribbon of 1mm of width and for four different value of applied DC field. (a) H=00 Oe, (b) H=1 Oe, (c) H=3 Oe, (d) H=9 Oe

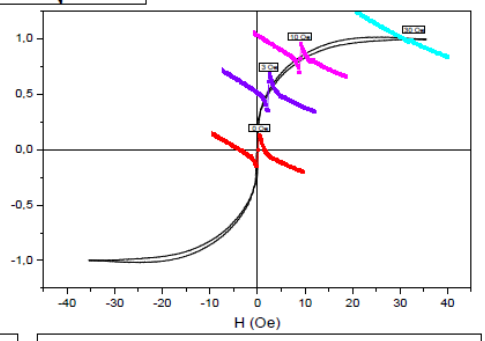

Fig 2: Hysteresis loops of a 3.5 cm length of glass coated microwire (dm=60um, Dgl= 100um) and resonance frequency evolution

[1]P. Marín, M. Marcos and A. Hernando.*Appl. Phys* **96**, 262512 (2010)
[2] C. Herrero-Gomez, P. Marın, and A. Hernando. *Appl. Phys* . **103**, 142414 (2013)
[3] Yating Chai et al. 978-1-4673-5221-5/13/IEEE (2013)
[4]Alfredo García-Arribas, Soft magnetic materials: from microsensors to cancer therapy, (2017).
[5]Keith T. Loiselle and Craig A. Grimes, Rev. Sci. Instrum., Vol. 71, No. 3, March 2000
[6] Craig A. Grimes1 et al. *Sensors* **2002***, 2,* 294-313

24. Indirect Dark Matter searches in the gamma-ray band and development of new analysis techniques for ground-based gamma-ray astronomy

Tjark Miener

The nature of dark matter (DM) is still an open question for modern physics. In the particle DM paradigm, this elusive kind of matter cannot be made of any of the known particles of the Standard Model (SM). Many efforts have been made in order to model the nature of the DM. Among others, and beyond the SM of particle physics, we focus on one part of this contribution on brane world theory as a prospective framework for DM candidates. Branons are new degrees of freedom that appear in flexible brane-world models corresponding to brane fluctuations. They are a natural DM candidate, because branons behave as weakly interacting massive particles (WIMPs), that are one of the most favored candidates for DM. Imaging atmospheric Cherenkov telescopes (IACTs) and other gamma-ray observatories could potentially detect DM indirectly, by observing secondary products of its annihilation into SM particles. In the past years, separate limits on the velocity-weighted cross section of DM self-annihilation have been produced by the Fermi-LAT, HAWC, H.E.S.S., MAGIC, and VERITAS collaborations. On the second part of this contribution, we will report on an initiative aiming at combining data from these five experiments in order to maximize the sensitivity of DM searches towards dwarf spheroidal galaxies (dSphs). We developed a python package, called LikelihodCombiner, which is able to produced combined limits. On the third part of this contribution, we present an alternative way of proceeding IACT data. IACTs capture images of the air showers, originated by the absorption of gamma rays and cosmic rays by the atmosphere, through the detection of Cherenkov photons emitted in the shower. One of the main factors determining the sensitivity of IACTs to gamma-ray sources in general is how well reconstructed the properties of the primary particle triggering the air shower are. We present how deep convolutional neural networks (DCNs) are being explored as a promising method for IACT event reconstruction, and illustrate it with some preliminary results obtained with CTLearn, a package for IACT event reconstruction through deep learning. Any improvement in the sensitivity of IACTs can be directly applied to indirect DM searches.

25. PET Imaging and Dose correlation from Proton Activation

Víctor Valladolid-Onecha

Range verification techniques for protontherapy include positron-emission tomography (PET) and prompt-gamma (PG) imaging. The main challenges preventing their clinical implementation are, in case of PET, the relatively long half-lives of the isotopes of interest and the large energy needed to activate PET-decaying nuclei [1].
We have investigated the use of certain isotopes as contrast agents for PET, increasing their activation rates and shifting the activity peaks towards the Bragg peak. For this purpose we have developed an activation calculation tool in different software packages such as TOPAS and PenH, and we have compared both. The results show an increased PET activation at the distal end of a 150 MeV proton beam, within 1 mm from the Bragg peak (BP), using Water-18O (H2O18) as a contrast agent.
The activation maps of 18F (T1/2≈110 min) and 15O (T1/2≈122 s) obtained from TOPAS and the SuperArgus 4R preclinical PET scanner [2] have been simulated with PeneloPET [3], in order to obtain 5-minute-long acquisitions right after irradiation and 15 minutes later. Results show the dominance of the 15O signal in a delocalized region far from BP in the first 5 minutes, but the BP distal end is perfectly identified for the 15 minutes delayed acquisition due to the 18F signal arising from the proton activation of 18O. The H2O18 is perfect for validation and verification with phantoms, and *in vivo* patients, provided if it could be biologically fixed in area of maximum dose deposition.

[1] S. España, et al., “The reliability of proton-nuclear interaction cross-section data to predict proton-induced PET images in proton therapy”, Phys. Med. Biol., 56(9) 2687–2698, 2011.

[2] S. España, et al., “PeneloPET, a Monte Carlo PET simulation tool based on PENELOPE: features and validation,” Phys. Med. Biol., 54 (6) 1723–1742, 2009.

[3] J. M. Udías, et al., “Performance evaluation of the PET subsystem of the extended FOV SuperArgus 6R preclinical scanner,” IEEE NSS MIC, 2018.